Final Draft
of the original manuscript:

Hanke, S.; Lemos, G.V.B.; Bergmann, L.; Martinazzi, D.; dos Santos, J.F.; Strohaecker, T.R.:

Degradation mechanisms of pcBN tool material during Friction Stir Welding of Ni-base alloy 625

In: Wear (2017) Elsevier

DOI: 10.1016/j.wear.2017.01.070

Degradation mechanisms of pcBN tool material during Friction Stir Welding of Ni-base alloy 625

S. Hanke[1], G.V.B. Lemos[2], L. Bergmann[1], D. Martinazzi[2], J.F. dos Santos[1], T.R. Strohaecker[2]

[1]Helmholtz-Zentrum Geesthacht, Institute of Materials Research, Materials Mechanics, Solid State Joining Processes, Max-Planck-Straße 1, Geesthacht, Germany

[2]Post-graduation Program in Mining, Metallurgical and Materials Engineering (PPGE3M), Federal University of Rio Grande do Sul (UFRGS), Porto Alegre, Brazil

Abstract

In Friction Stir Welding (FSW), interactions between the plasticized stirred material and the tool significantly affect resulting weld properties. When welding metals with high strength and melting point, the tribological load on the tool is severe, and poses the main limiting factor for the technology's industrial exploitation. Since tool materials are loaded to their limits, it is essential to understand the interactions of specific tool material and welded metal combinations.

In the present study 3.2 mm alloy 625 sheets were joined using a pcBN tool with W-Re binder phase. Wear lead to a change in tool geometry followed by tool fracture. In SEM investigations the welds revealed typical banded structures, composed of small grains and non-metallic phases containing W from the tool material. The tool surface is extensively covered by adhering sheet metal. Further, BN grain pull-outs and appearances of diffusive wear are visible on the worn tool surface.

Tool wear is mainly caused by detachment of BN grains due to thermal softening of the metallic binder phase and dissolution of BN in the hot material in the stirred zone. Using low rotational speeds resulting in lower process temperatures reduces tool wear and results in a homogeneous stirred zone.

Keywords: Inconel 625, engineering ceramics, high temperature, manufacturing processes

1 Introduction

Friction Stir Welding (FSW) is to date mainly applied to low melting point alloys, due to the difficulty of finding adequate tool materials resisting the high thermal, chemical and mechanical loads associated with the welding of high melting point materials. Persistent research and development efforts are made to find a satisfactory solution to this challenge, because the FSW process poses several advantages, amongst others with regard to

improved weld properties, reduced distortion and the avoidance of spatter and emissions [1] [2].

The feasibility of applying FSW to the austenitic Ni-base alloy 625 and the obtained joint properties have been investigated recently [3] [4]. This application is of particular interest for the oil and gas industry, where this alloy is used for its corrosion resistance. Since alloy 625 is predominantly strengthened by alloying elements in solid-solution, FSW is prone to provide good joint properties. In solid-state joining processes, burn-off of alloying elements, which would be detrimental to the corrosion properties, is avoided. Further, a reduction of mechanical strength due to alterations of precipitates is of little relevance, and solid-solution strengthening is not affected by FSW.

While mild steel can be friction stir welded with low tool wear [5], particularly Ti-6Al-4V and austenitic alloys, as is alloy 625, lead to significant degradation, due to very high process temperatures [6], and the maintaining of high strength at elevated temperatures [7].

Tool materials frequently used for FSW of high melting point materials include cemented carbides, mainly WC-Co [3] [6] [8], polycrystalline cubic Boron Nitride (pcBN) [7] [8] [9], refractory metal alloys based on W [8] [10] [11], intermetallic alloys [12] as well as ceramics [8] [13]. pcBN is a preferred tool material for FSW of high strength alloys, owing to its high strength and hardness at elevated temperatures, along with high temperature stability. Furthermore, the specific interaction of pcBN with the plasticized sheet material results in a smooth weld surface [14].

The tool material and its properties affect the FSW process and the obtained weld in various aspects. The tool geometry determines the heat generation, material flow and the required process parameters, and at the same time influences the stresses acting on the tool. Important properties of the tool material include thermal conductivity and heat capacity, mechanical strength at elevated temperatures and the ability to resist thermal cycling. Furthermore, the interaction between the tool surface and the welded metal influences the process through the acting friction and adhesion, as well as tool wear. All these mentioned properties can have an impact on the resulting joint properties and microstructure [10] [11] [14].

Ni-base alloys have considerable high temperature strength [15] and therefore a strong mechanical interaction with the tool surface can be expected, as it is observed in machining processes [16]. Within the stirred zones of FSW joints in alloy 625 [3], tungsten (W) was measured in banded structures of low grain size, and explained by wear from the used WC-Co tool. Similarly, in [17] a region of low grain size inside the stir zone containing small BN wear particles was found when a pcBN tool was used to weld Ni-base alloy 600. It was concluded that grain growth during cooling was locally prevented by the presence of the particles on grain boundaries [17].

In the scope of the present work, FSW was applied to the Ni-base alloy 625 using a pcBN tool with W-Re binder phase. Since no study of this particular combination of tool and welded material was found in literature, initial process parameter development based on published data of similar materials was carried out [18]. In the process of establishing suitable welding parameters, significant tool wear was observed. The main objectives of the current study were to investigate the wear mechanisms of the tool, as well as the effects of the wear on the joint microstructure. Additionally, this investigation intended to determine if wear can be reduced or avoided through the choice of adequate welding parameters.

2 Experimental Procedure

3.2 mm thick sheets from Ni-base alloy 625 were used in this study. The chemical composition given by the supplier's certificate is presented in Table 1, and is in accordance with the range prescribed in the German DIN 17744:2002-09 standard [19].

	Cr	Fe	Mo	Nb	Co	Mn	Al	Ti	Si	C	Ni
alloy 625	21.7	4.7	8.6	3.4	0.03	0.09	0.13	0.18	0.18	0.015	bal.

Table 1: Chemical composition of the welded sheet material (weight-%).

Light grinding of top and adjoining sheet surfaces to remove oxides and contaminants was performed using grid emery cloth. This preparation of surfaces was noted, during the first welding trials, to be an important step to improve weld surface quality. Directly before welding the surfaces were cleaned using ethanol.

FSW was carried out on a custom built Gantry machine fitted with servomotors, data acquisition (forces in 3D, torque and position of each axis), and automated control systems. The threaded pcBN tool with W-Re binder phase used in this study had a shoulder diameter of 25 mm and a probe length of 3 mm. The tool, sold under the specification Q70, is claimed by the supplier (MegaStir, Provo, Utah, USA) to have the highest available toughness, and is therefore recommended for use on high-strength stainless steels and Ni-base alloys [20].

The FSW tool was tilted 1.5° forward from the vertical axis and Argon shielding surrounding the tool during welding was utilized to minimize surface oxidation. The welding direction was parallel to the rolling direction of the alloy 625 sheets.

In the scope of the conducted welding study two groups of process parameters were applied, distinguished by high and low rotational speeds, as shown in Table 2. First welding trials using high rotational speeds (welds I, II, III and IV) were not satisfactory, showing an irregular, rough top surface appearance of the joints along the complete welded length of 500 mm. Further attempts using low rotational speed (welds V and VI) were successful, reaching a very smooth and homogeneous weld top surface appearance, and defect free

joints. During the attempt to decrease the rotational speed further, from 200 to 150 min^{-1} (weld VII), the tool fractured after only 50 mm of weld length, due to an increase in process torque. The torque rises with decreasing rotational speed, e.g. it was 30 Nm in weld III, 110 Nm in weld VI, and increased to more than 120 Nm during weld VII. All the joints showed a lack of penetration, since the probe was shorter (3 mm) than the sheet thickness (3.2 mm). This discrepancy was further increased during the welding trials due to wear induced shortening of the tool probe.

		traverse speed [mms^{-1}]	axial force [kN]	rotational speed [min^{-1}]	weld surface quality	welded length [mm]
high rotational speed	I	1	50	500	poor	500
	II	1	50	600	poor	500
	III	1	60	1200	medium	500
	IV	1	60	1000	medium	500
low rotational speed	V	1.5	60	200	good	250
	VI	1	60	200	excellent	250
	VII	1	60	180	good	50

Table 2: Welds carried out in the current study with the investigated pcBN tool. Tool fracture occurred after 50 mm into weld number VII.

Cross sections from the welded sheets were prepared by standard metallographic methods, including mechanical grinding and polishing down to 1 µm grain size diamond polishing suspension. The samples were etched using Adler solution (25 ml distilled water, 50 ml hydrochloric acid, 15 g Fe(III) chloride, 3 g ammonium tetrachlorocuprate) to reveal the microstructure. Both weld cross sections and the worn tool surface were examined by scanning-electron-microscopy (SEM; Quanta FEG 650, FEI Europe B.V., Eindhoven, The Netherlands) and energy dispersive X-ray spectroscopy (EDS; Apollo X-SDD, EDAX Inc., Mahwah, NJ, USA).

3 Results

3.1 Weld Microstructure

The top view of the weld presented in Figure 1 (a) shows the good weld surface obtained with low rotational speed, smooth and without annealing colors. Still, this weld was terminated by tool fracture, and some tool fragments are visible in the exit hole. Metallographic cross sections from welds carried out at high (III) and low (VI) rotational speeds are presented in Figure 1 (b) and (c), and show distinct differences. The stir zone (SZ) of weld III is deeper than that of weld VI, which is mainly due to tool wear during the welds carried out in between. A contribution of the different welding parameters to the activation of different material volumes in the two welds is also possible. The SZ of weld III appears to be narrower, especially close to the sheets' top surface (Figure 1 (b)). This is due the fact

that under this welding parameter set a sharp transition between recrystallized (dark etching) material and the surrounding, only heat affected or slightly deformed material can be observed. Close to the sheets' surface a narrow material volume of approximately 100 µm depth is recrystallized, which is not recognizable in the presented low magnification optical microscope images. Throughout the SZ bands of varying dark shading are recognizable. In weld VI the SZ is of homogeneous appearance with only a banded, dark etching region at the advancing side (AS) close to the weld surface. Particularly the retreating side (RS) of weld VI shows a continuous, instead of a sharp transition to the surrounding material (Figure 1 (c)).

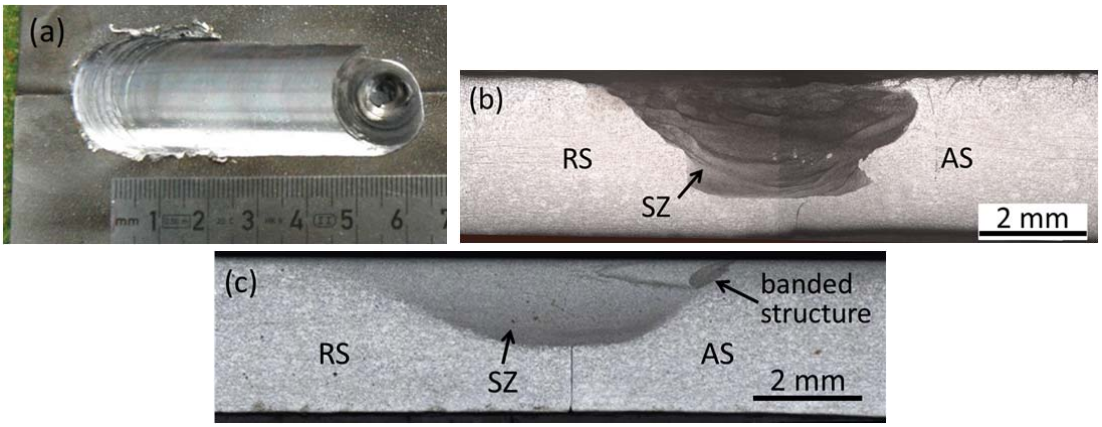

Figure 1: Top view of weld VII in alloy 625, ended due to tool fracture (a), and cross section showing SZ and dark etching banded structure of weld III (b) and weld VI (c).

In Figure 2 results of the SEM investigation of the SZ of weld III are presented. In the images of the etched microstructure equiaxed grains are recognizable, with a size of 5.6 ± 1.8 µm. A phase different from the solid-solution grains is present extensively along the grain boundaries, with blocky or lamellar shapes (Figure 2 (b)). In the locations indicated by numbers *1 and *2, EDS measurements were taken, the results of which are given in the table in Figure 2 (c). The chemical composition in the grain interior (point *2) corresponds well with the composition given by the supplier (compare Table 1), with an increased content of C and N. The latter must be considered cautiously due to the inaccuracy of the EDS technique with regard to light elements, and its sensitivity to surface contamination from the environment. Still, the measurement taken on the grain boundary phase displays a higher C content and no N was detected here. Further, the Cr, Nb and Mo content is increased in this location, at the expense of Ni. W was additionally detected, which is not originally present in the alloy 625 used for this study.

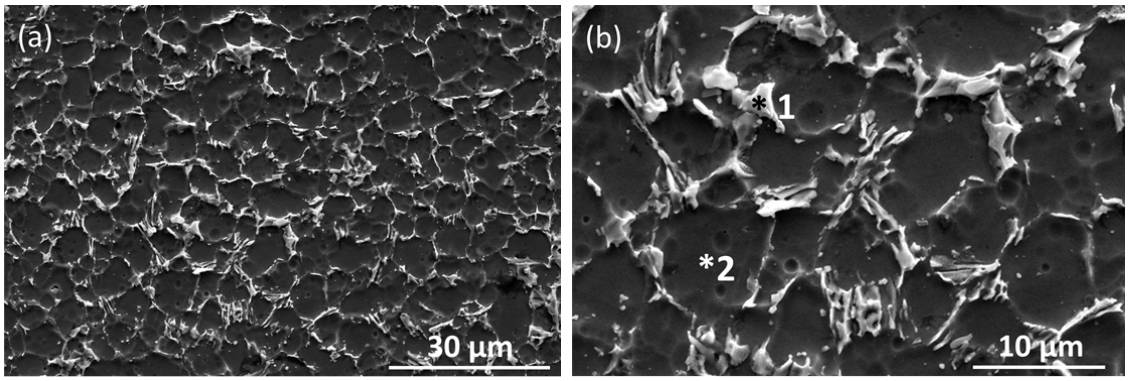

(c)	C	N	Cr	Fe	Ni	Nb	Mo	W
*1	7.3	-	22.4	3.0	35.0	6.9	22.7	2.7
*2	2.1	1.6	21.7	5.0	59.5	3.0	7.1	-

Figure 2: SEM image from SZ of weld III displaying an additional phase on the boundaries of equiaxed recrystallized grains (a); higher magnification with indicated locations of EDS measurements (b); results of EDS measurements in weight-% (c).

3.2 Tool Wear

The pcBN tool used for the welds in this study showed obvious signs of wear, and a continuous reduction of the probe diameter and length was observed. In Figure 3 (a) the tool is shown after accomplishing all welds listed in Table 2, showing adhering sheet material oxidized to a golden color, as well as the fractured probe. The detached tool fragment was further analyzed by SEM, and in Figure 3 (b) a secondary electron image showing part of the probe and the shoulder is presented. The very bright spots on the shoulder stem from the W-Re binder phase in the tool material, due to its high density. On the probe surface these bright regions are not visible, because it is extensively covered by alloy 625 material.

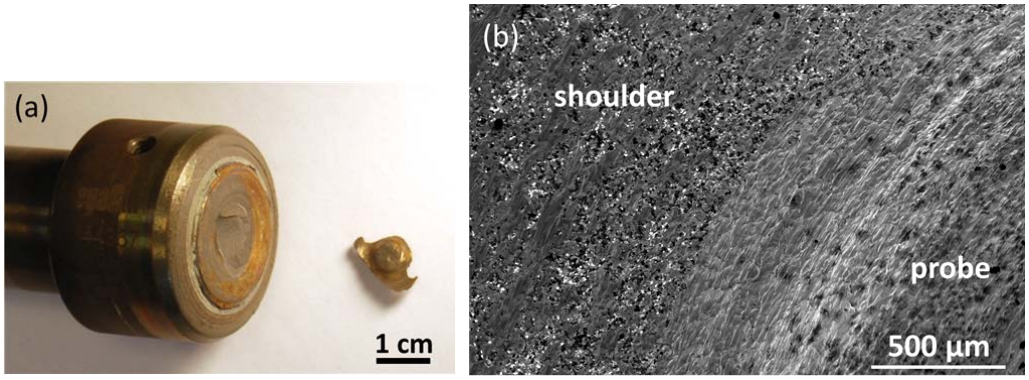

Figure 3: Worn tool after fracture (a) and SEM image of detached tool fragment showing probe completely and shoulder partially covered with sheet material (b).

The adhering metal displays a scale-shaped morphology (Figure 4 (a)), with local appearances of solidification (porous regions) and oxidation (darks regions). Also locally the grain boundaries of the adhering alloy 625 are visible. The tool shoulder is not covered by sheet material to the same extend. Instead, the adhering metal is present in the shape of stripes, between which the worn tool material is visible (Figure 3 (b)). In Figure 4 (b) the worn tool surface as well as adhering sheet material are visible. Darker regions mainly in the center and the left of the image are BN grains, with partially smooth and partially rough, blurry surface appearance. On the latter the EDS measurement *1 (Figure 4 (b)) was located, and a chemical composition of mainly B and N was detected, with small amounts of O and W. Converting the values to atomic-%, they equal to 50.2 at% B and 47.0 at% N, which is close to the ideal ratio of 1:1 in BN crystals. Although the EDS technique is often unreliable in measuring light elements, the results are reasonable and imply a good accuracy of the measurement in the present case. The brighter region towards the upper left corner of the image, which contains the EDS measurement spots *2 and *3, is the W-Re binder phase of the tool material. The shape of detached BN grains is still visible on the W-Re islands, due to flat regions with a porous appearance. The chemical composition of such a region was determined by measurement *2, and consists mainly of W, with approximately 30 wt% Re and a small addition of Al. Several wt% of O and N were also frequently detected (Figure 4 (c)). Crystals protruding from the porous areas of W-Re were found to consist mainly of W, with no detectable amount of Re, as seen in the measurement *3 in Figure 4. Here, also a high O content was found in addition to low amounts of elements from the welded metal. The material in the measurement location *4 stems clearly from the sheets, and some traces of tool material as well as O and C were additionally detected.

4 Discussion and Conclusions

From the appearance of the metallographic cross sections it is obvious, that a significant difference exists in the material flow in alloy 625 friction stir welds at high and low rotational speeds. It can be assumed, that the process temperatures reached at high rotational speed were very high, which was also observed in the glowing colors during welding. Such high temperatures may result in material flow localization at the tool surface, where the heat is generated. This corresponds to the narrow shape of the SZ and the sharp boundaries to the surrounding material (Figure 1 (b)), as well as the low torque values. Considering that also the relative speed between the tool surface and the stirred metal is high under such process parameters, the localized material flow must have occurred also at fast deformation (flow) rates. The wider SZ of the weld generated at low rotational speed (weld VI), with a dark etching region on the AS, presents the typical appearance of austenitic alloys after FSW, as reported in literature [7] [11].

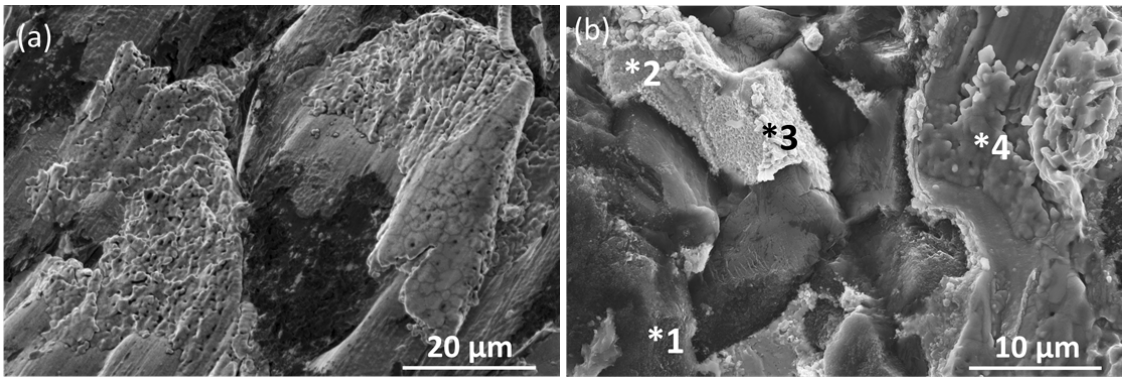

(c)	B	C	N	O	Al	Cr	Fe	Ni	Nb	Mo	W	Re
*1	43.9	-	53.2	2.0	-	-	-	-	-	-	0.9	-
*2	-	-	5.3	4.5	0.8	-	-	-	-	-	33.1	56.3
*3	-	-	3.9	24.8	-	1.3	-	2.7	-	-	67.3	-
*4	-	2.3	-	4.4	-	19.9	4.6	55.4	2.8	7.5	3.1	-

Figure 4: Sheet material adhering to the tool probe in the shape of scales, showing grain boundaries, solidified regions (porous) and oxidation (dark) (a); worn tool shoulder surface displaying deteriorated BN grains (*1), binder phase (*2 and *3) and adhering sheet material (*4), the numbers indicating locations of EDS measurements (b); EDS results in weight-% (c).

The localized material flow at high process temperatures under high rotational speed causes severe tool wear. While in [7] the formation of Borides was found through transmission-electron-microscopy investigations in FSW joints of stainless steel produced with a pcBN tool, in the current study mainly W was detected in the alloy 625 stirred zone. It is still possible that dissolved B is present below the detection limit of the EDS measurements. At the high rotational speed, the observed grain boundary phase contained mainly refractory metal elements from alloy 625 and the tool material together with an increased C content, indicating the formation of carbides. Since they are large, partially of lamellar shape and appear to be located on the grain boundaries of the equiaxed, recrystallized alloy 625 grains, it is reasonable to assume that they have grown to this size during cooling (Figure 2).

The sheet material adhering to the tool surface, showing scales and signs of solidification, was left there from the last weld, which was conducted at low rotational speed. Still, obviously very high temperatures were reached, locally above the melting range of alloy 625. The worn tool surface shows pull-outs of BN grains, recognizable from locally smooth surfaces of the binder phase and remaining BN grains. In other locations, close to adhering sheet material, the BN grains show rough surfaces due to thermal and/or chemical deterioration.

From findings reported above, at least two mechanisms of wear can be identified. On the one hand, diffusion occurs between BN and the adhering, hot sheet material, thereby

dissolving parts of the BN crystals in the alloy 625 matrix. This diffusive wear mechanism has also been described for FSW of stainless steel [7], and is also known from machining Ni-base alloys using cBN cutting tools [21]. On the other hand, BN grain pull-outs represent a mechanical type of wear. Still, wear seems to be more severe at high rotational speeds resulting in relatively lower torque, implying a less severe mechanical interaction between the stirred metal and the tool surface. This behavior may be related to the chosen metallic binder phase. While it brings about the advantage of a higher toughness compared to a ceramic binder phase, it undergoes thermal softening at elevated temperatures. Particularly at the high rotational speeds, a decreased strength of the binder phase due to the high temperatures may have contributed to severe tool wear through grain pull-outs. The final tool failure eventually occurred due to the decreased cross section of the remaining tool material, and the high torque during the last weld.

It can be concluded that tool wear must be expected when joining alloy 625 by FSW using a pcBN tool with W-Re binder phase. It may be kept to an acceptable level, when high process temperatures are avoided. The effect of the fast material flow around the tool at high rotational speed due to shear localization remains to be clarified, e.g. by applying low rotational speeds and reducing the welding speed, which will also increase the process temperature. In this way a different material flow behavior may be achieved, and tool wear could be investigated under such conditions. Generally, when processing alloys with a tendency for shear localization, sudden or local changes in the material flow stress and their potential effects on tool wear must be taken into account when varying the process parameters. In order to maintain a stable process, such variations should be avoided.

5 Acknowledgements

The authors of this work would like to thank CNPq (National Council for Scientific and Technological Development) through the Science Without Borders program and CAPES (Brazil) for their support.

6 References

[1] R.J. Steel, Q. Liu, M. Collier, J. Peterson, R. Rowland, S.M. Packer, Friction Stir Welding: New Developments for Oil and Gas Industry. In: International Oil and Gas Conference and Exhibition in China. Society of Petroleum Engineers, Beijing, China (2010).

[2] J. de Backer, M. Soron, Three-dimensional friction stir welding of Inconel 718 using the ESAB Rosio FSW-robot. In: Trends in Welding Research Conference. Chicago, IL, USA (2012).

[3] K.H. Song, K. Nakata, Mechanical properties of friction-stir-welded Inconel 625 alloy, Materials Transactions 50/10 (2009) 2498-2501.

[4] K.H. Song, K. Nakata, Effect of precipitation on post-heat-treated Inconel 625 alloy after friction stir welding, Materials and Design 31 (2010) 2942-2947.

[5] Z. Iqbal, A.N. Shuaib, F. Al-Badour, N. Merah, A. Bazoune, Microstructure and hardness of friction stir weld bead on steel plate using W-25%Re pin tool, In: Proceedings of the ASME 2014 12th Biennial Conference on Engineering Systems Design and Analysis ESDA2014, Copenhagen, Denmark (2014).

[6] J. Wang, J. Su, R.S. Mishra, R. Xu, J.A. Baumann, Tool wear mechanisms in friction stir welding of Ti-6Al-4V alloy, Wear 321 (2014) 25-32.

[7] S.H.C. Park, Y.S. Sato, H. Kokawa, K. Okamoto, S. Hirano, M. Inagaki, Boride formation induced by pcBN tool wear in friction-stir-welded stainless steels, Metallurgical and Materials Transactions A 40A (2009) 625-636.

[8] Y.S. Sato, M. Muraguchi, H. Kokawa, Tool wear and reactions in 304 stainless steel during friction stir welding, Materials Science Forum 675-677 (2011) 731-734.

[9] J. Rodriguez, A.J. Ramirez, Microstructural characterization of friction stir welding joints of mild steel to Ni-based alloy 625, Materials Characterization 110 (2015) 126-135.

[10] B. Thompson, S.S. Babu, Tool degradation characterization in the friction stir welding of hard metals, Welding Journal 89 (2010) 256-261.

[11] S.S. Kumar, N. Murugan, K.K. Ramachandran, Influence of tool material on mechanical and microstructural properties of friction stir welded 316L austenitic stainless steel butt joints, International Journal of Refractory Metals and Hard Materials 58 (2016) 196-205.

[12] Y. Azuma, Y. Kameno, T. Takasugi, Friction stir welding in stainless steel sheet of type 430 using Ni-based dual two-phase intermetallic alloy tool, Welding International 27/10-12 (2013) 929-935.

[13] Y. Kim, I. Kim, J. Kim, J. Park, Mechanical properties and tool life of friction-stir-welded DP590 using the Si_3N_4 tool, Materials Transactions 55/10 (2014) 1557-1563.

[14] R. Rai, A. De, H.K.D.H. Bhadeshia, T. DebRoy, Review: friction stir welding tools, Science and Technology of Welding and Joining 16/4 (2011) 325-342.

[15] N. Srinivasan, Y.V.R.K. Prasad, Hot working characteristics of nimonic 75, 80A and 90 superalloys: a comparison using processing maps, Journal of Materials Processing Technology 51 (1995) 171-192.

[16] M.A. Rodrigues, A. Hassui, R.H. Lopes da Silva, D. Loureiro, Tool life and wear mechanisms during alloy 625 face milling, International Journal of Advanced Manufacturing Technology DOI 10.1007/s00170-015-8056-4.

[17] Y.S. Sato, P. Arkom, H. Kokawa, T.W. Nelson, R.J. Steel, Effect of microstructure on properties of friction stir welded Inconel Alloy 600, Materials Science and Engineering A 477 (2008) 250-258.

[18] G.V.B. Lemos, L. Simoni, L. Bergmann, D. Souza, D.B. Araujo, J.F. dos Santos, T.R. Strohaecker, R.M. Schroeder, Caracterização Preliminar da Microestrutura em Cordões de Solda da liga 625 produzidos através dos processos de SFMM e MIG. In: XLI CONSOLDA - CONGRESSO NACIONAL DE SOLDAGEM, Salvador, Bahia, Brazil (2015).

[19] DIN 17744:2002-09. Wrought nickel alloys with molybdenum and chromium - Chemical composition (2002) Beuth Verlag GmbH, Berlin, Germany.

[20] website: http://www.slb.com/services/megastir/products/high_temp/q_series.aspx (August 14, 2016)

[21] D. Zhu, X. Zhang, H. Ding, Tool wear characteristics in machining of nickel-based superalloys, International Journal of Machine Tools & Manufacture 64 (2013) 60-77.